Extracting continuum information from $\Psi(t)$ in time-dependent wave-packet calculations

L. B. Madsen, L. A. A. Nikolopoulos,* T. K. Kjeldsen, and J. Fernández
Lundbeck Foundation Theoretical Center for Quantum System Research, Department of Physics and Astronomy, University of Aarhus, 8000 Aarhus C, Denmark

(Received 1 October 2007; published 18 December 2007)

The theory of measurement projection operators in grid-based time-dependent wave-packet calculations involving electronic continua in atoms and molecules is discussed. A hierarchy of projection operators relevant in their individual restricted configuration spaces is presented. At asymptotically large distances from the scattering or interaction center the projection operators involve plane waves only. To reach this asymptotic regime, however, large propagation times and large boxes may be required. At somewhat smaller distances from the scattering center, the projection operators are expressed in terms of analytical single-center Coulomb scattering waves with incoming wave boundary conditions. If propagation of the wave packet to these asymptotic regimes is impeded, the projection operators involve the exact scattering states which are not readily available in the wave-packet calculation and hence must be supplied by an additional, typically very demanding, calculation. The present approach suggests an exact way of analyzing the timely problem of the one-electron continuum in nonperturbative calculations. A key feature is that the propagated wave packet includes every interaction of the full Hamiltonian. The practicality of the proposed method is illustrated by the nontrivial example of strong-field ionization of the molecular hydrogen ion. Finally, the extension of the presented ideas to single and double ionization of two-electron systems is discussed.

DOI: 10.1103/PhysRevA.76.063407 PACS number(s): 32.80.Rm, 33.80.Rv, 31.15.−p, 02.70.Hm

I. INTRODUCTION

In many *ab initio* approaches to dynamics in atomic, molecular, and optical physics the time-dependent Schrödinger equation is solved in coordinate space. The result of such an approach is the space representation of the state of the system, $\langle\{\boldsymbol{r}\}|\Psi(t)\rangle=\Psi(\{\boldsymbol{r}\},t)$, where $\{\boldsymbol{r}\}$ denotes generally the set of coordinates involved. In practice, such wave packet approaches have been successfully applied to the strong-field ionization of atoms and molecules within the single-active-electron approximation (see, e.g., the reviews [1–3]) and in collisions (see, e.g., Ref. [4]). In all cases, one of the theoretical tasks is to relate the theoretical description in terms of the wave packet $\Psi(\{\boldsymbol{r}\},t)$ to the experimental observables of the system. Restricting for clarity the discussion to the case of a single active electron, the most specific information in strong-field ionization is the momentum-resolved ionization probability $dP/d\boldsymbol{k}$, i.e., the fully differential ionization probability (for a fixed orientation of the nuclei in the molecular case) for ionization into the momentum interval $[\boldsymbol{k};\boldsymbol{k}+d\boldsymbol{k}]$. Of course it has been known since the early works on scattering theory how to obtain this quantity by squaring the projection of $\Psi(\boldsymbol{r},t)$ on the exact scattering state $\psi_{\boldsymbol{k}}^{-}(\boldsymbol{r})$ that asymptotically, at large distances, acquires the momentum $\boldsymbol{k}$ [5]. There is one major practical problem here: The scattering states are only known exactly analytically for the pure single-center Coulomb problem and generally it is a demanding task to construct these states numerically from first principles even for the simplest systems such as He, H_2^+, and H_2 [6,7]. It should be noted that quantities of a more integral nature can be determined without making a projection. For example, the total ionization probability, P, can be determined by keeping track of the wave-function norm absorbed by an absorbing boundary. The angular ionization probability, $dP/d\Omega$, can be obtained by the analysis of the radial flux in direction $\hat{\boldsymbol{k}}$ (see, e.g., Refs. [8–10] and Sec. VI below). The photoelectron spectrum dP/dE can be obtained by a spectral analysis of the autocorrelation function of $\Psi(\boldsymbol{r},t)$ [11,12], with $E=k^2/2$ the electron energy. This method extended previous bound state analysis [13,14] to the continuum. Yet an alternative approach for the analysis of the physics of the final state has been to divide the configuration space into different regimes and associate the electron density in a particular region with ionization (see, e.g., Refs. [15,16]). As noted, e.g., in Ref. [17], clearly, the fixation of these boundaries is associated with a certain degree of arbitrariness.

It is the purpose of the present work to point out that the availability of the wave packet $\Psi(\boldsymbol{r},t)$ in space and as a function of time (in particular at instants of time $t=t_0+T$ later than the end of the time-dependent interaction, t_0) may lead to tremendous simplifications in the analysis of the measurable content of the wave packet. All the information about the short-range interaction, i.e., phase shifts, and possible channel mixing, e.g., between different angular momentum states in the case of a nonspherical symmetric molecule, is fully contained in $\Psi(\boldsymbol{r},t)$ allowing for the analysis of the scattering content by the application of simple asymptotic projection operators in the long-time limit (see Fig. 1). Although the time-dependent interaction, inducing the transition into the continuum, can be of general type, we make the discussion explicit and refer to ionization by an intense laser pulse of short duration in the following.

The paper is organized as follows. In Sec. II, the analysis of the scattering content of $|\Psi(t)\rangle$ at time t_0 just after the end

*Present address: Department of Applied Mathematics and Theoretical Physics, The Queen's University of Belfast, Belfast, BT7 1NN, Northern Ireland, UK.

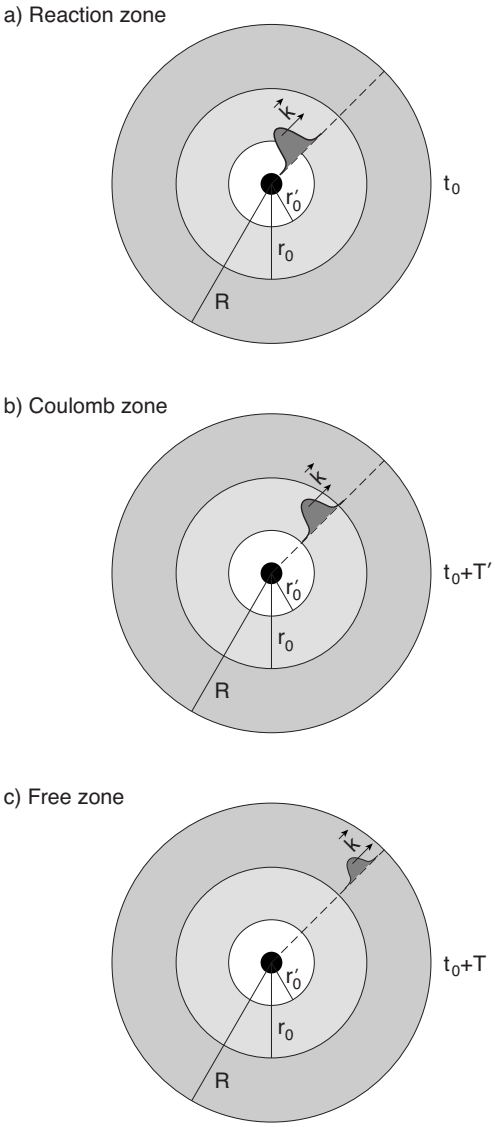

FIG. 1. Separation of configuration space into spatial zones with each of their characteristic Hamiltonian. The features moving away from the scattering center going from (a) to (c) illustrate a component of the wave packet moving with central momentum $\boldsymbol{k}$. In (a), the wave-packet component moving away is shown just after the end of the pulse at time t_0. The spatial region corresponding to this situation we refer to as the reaction zone and discuss it in Sec. II. In (b), an additional time T' has passed and the packet is at intermediate distances $r_0' < r < r_0$, where the Coulombic monopole from the scattering center dominates. This situation we refer to as the Coulomb zone and discuss it in Secs. V–VII. In (c), the time T has passed by since the end of the pulse, and the packet is in the free zone at asymptotic large distances, $r > r_0$. In neutral atomic and molecular systems the situation in (c) is, in a strict theoretical sense, not encountered since the Coulomb tail of the potential gives a logarithmic phase distortion of the plane-wave asymptotic state at all distances. We include (c), since it is of relevance in negative ions (and other branches of physics). We discuss the projections corresponding to (c) in Sec. IV. The radius **R** denotes the boundary of the sphere defining the part of space that is accounted for in a numerical calculation. In practical calculations, to prevent reflection from the boundary, an absorbing boundary may be used.

of the pulse is discussed in the case of a one-electron wave packet [Fig. 1(a)]. In Sec. III, we present some formal and mathematical details which prove firmly the validity of the present approach based on asymptotic projection operators. In Sec. IV, we discuss how to perform the analysis in the asymptotic free-electron zone at times t_0+T, where T is chosen such that all momentum components of interest have reached the asymptotic regime [Fig. 1(c)]. In Sec. V, we discuss how to do the analysis in the somewhat closer regime where the Coulombic monopole dominates: The Coulomb zone [Fig. 1(b)]. In Sec. VI we compare numerical results on strong-field ionization of H_2^+ obtained by projection on exact scattering states and with projection in the Coulomb zone at times $t=t_0+T'$ and illustrate the accuracy and practicality of the method. In Sec. VII, we discuss an extension of the present ideas to the two-electron system: Single-ionization and excitation, as well as double ionization. In Sec. VIII, the main conclusions are presented.

Atomic units ($m_e=\hbar=e=1$) are used throughout unless stated otherwise.

II. SCATTERING ANALYSIS JUST AFTER THE END OF THE PULSE

When the short intense laser pulse has ended at time t_0, the time-dependent wave packet $\Psi(\boldsymbol{r},t)$ given in terms of complex amplitudes in points in space is available in a theoretical grid-based calculation. Though not readily at hand in this case, the wave packet may formally be thought of as being represented by an expansion in a basis of energy eigenstates $\Psi(\boldsymbol{r},t)=\Sigma_n c_n \psi_n(\boldsymbol{r})\exp(-iE_n t)+\int d\boldsymbol{k} c_{\boldsymbol{k}} \psi_{\boldsymbol{k}}^-(\boldsymbol{r}) \times\exp[-i(k^2/2)t]$, with $H\psi_n(\boldsymbol{r})=E_n\psi_n(\boldsymbol{r})$, and where the expansion includes a sum over bound and an integral over continuum scattering states of the field-free Hamiltonian, H. It is clear that the probability of being in a particular eigenstate does not change in time once the driving pulse is over. The analysis of the scattering content of $\Psi(\boldsymbol{r},t)$ may therefore be performed immediately after the end of the pulse with the projection operator

$$\mathcal{P}_{\boldsymbol{k}} = |\psi_{\boldsymbol{k}}^-\rangle\langle\psi_{\boldsymbol{k}}^-|, \tag{1}$$

where $\psi_{\boldsymbol{k}}^-(\boldsymbol{r})$ is the momentum normalized, $\langle\psi_{\boldsymbol{k}}^-|\psi_{\boldsymbol{k}'}^-\rangle=\delta(\boldsymbol{k}-\boldsymbol{k}')$, scattering state that conforms with incoming-wave boundary condition and develops asymptotic momentum $\boldsymbol{k}$. Accordingly, the probability for ionization with asymptotic momentum $\boldsymbol{k}$ is $\mathrm{Tr}[\rho\mathcal{P}_{\boldsymbol{k}}]$, $\rho=|\Psi(t_0)\rangle\langle\Psi(t_0)|$, i.e.,

$$\frac{dP}{d\boldsymbol{k}} = |\langle\psi_{\boldsymbol{k}}^-|\Psi(t_0)\rangle|^2. \tag{2}$$

In scattering theory, $\psi_{\boldsymbol{k}}^-(\boldsymbol{r})$ is called the *out* or *outgoing* state. The advantage of this approach where the projection is performed with the exact scattering state is that no propagation of the wave packet is required after the end of the pulse, and compared with the methods discussed below it may hence pose less demands to the box size and avoid associated numerical problems in propagating the wave packet. An additional advantage is that the scattering states and the bound energy eigenstates making up the formal expansion of the

wave packet are solutions to the same field-free Hamiltonian. This means that eigenstates are orthogonal and the projection integral in Eq. (2) is readily performed over all space: No prior projecting out of any bound state part is necessary. Additionally, in Eq. (2) there is in principle nothing that favors particular $\boldsymbol{k}$ values, i.e., application of Eq. (2) is equally valid and "easy" for low, intermediate, and high $\boldsymbol{k}$ values. In practice, of course, the "easiness" will typically depend on the dimensions of the grid. The disadvantage in the resolution in Eq. (2) is that the analysis requires per default the exact scattering states of the Hamiltonian H, the construction of which in general is an elaborate affair. The hydrogen atom and hydrogenlike ions are the only cases where the scattering states are known analytically in terms of Coulomb wave functions. For atoms described in the single-active-electron approximation the scattering states can be found relatively simply numerically by exploiting the spherical symmetry of the problem. In molecules the multicenter character of the remaining molecular ion means that the angular momentum of the ejected electron is no longer a constant of motion and the construction of the scattering states becomes a multichannel problem in terms of angular momenta [7,18,19]. Hence, in general the scattering states have to be provided by an additional structure calculation typically performed in an eigenstate basis. This computational overhead is a clear disadvantage. In Sec. VI we find the scattering states for H_2^+ in a B-splines basis-state approach and compare the results with the asymptotic analysis in the Coulomb zone.

We note in passing that Eq. (2) as it stands is the natural starting point for analysis in the perturbative regime. For example, for perturbative single-photon ionization, the time-dependence drops out and essentially in Eq. (2) $|\Psi(t_0)\rangle \rightarrow \boldsymbol{\varepsilon}\cdot\boldsymbol{p}|\phi_0\rangle$, where $\boldsymbol{\varepsilon}$ is the polarization vector, $\boldsymbol{p}$ the momentum operator, and $|\phi_0\rangle$ the field-free initial bound state. In this case the perturbation introduces a transition between exact energy eigenstates of H and no wave packet is formed. Accordingly there is no possibility to propagate to asymptotic regions and perform the scattering analysis there. For femto- and attosecond pulses, however, the creation of a wave packet makes the approach of Secs. IV and V natural.

III. PROPERTIES OF THE *OUT* STATE AND IMPLICATIONS FOR THE SCATTERING ANALYSIS

A fundamental property of the out state $\psi_{\boldsymbol{k}}^-(\boldsymbol{r})$ is that it asymptotically acquires the momentum $\boldsymbol{k}$. Although this is well-known, we dwell a little on the way this is proved to be able to understand and describe clearly the implications in the present context.

We write the total field-free time-independent Hamiltonian $H=H_0+V$, where H_0 is assumed to be simple such that all its eigenstates $|\phi_n\rangle$ and eigenvalues E_n are known, i.e., $H_0|\phi_n\rangle=E_n|\phi_n\rangle$. Here the index n discriminates between different, possibly degenerate, channels. Following Ref. [20], we call the system with energies E_n and states $|\phi_n\rangle$ the *reference system*. The term V in H is the interaction that causes perturbations of the unperturbed reference system. We may find the stationary continuum states that solve the true problem including V, $(H-E_{\boldsymbol{k}})|\psi_{\boldsymbol{k}}^-\rangle=0$, at the particular energy $E_{\boldsymbol{k}}$ by the usual integral equation technique leading to the following Lippmann-Schwinger equation for $|\psi_{\boldsymbol{k}}^-\rangle$:

$$|\psi_{\boldsymbol{k}}^-\rangle = |\phi_{\boldsymbol{k}}\rangle + \lim_{\eta\to 0^+} \frac{1}{E_{\boldsymbol{k}} - H_0 - i\eta} V|\psi_{\boldsymbol{k}}^-\rangle, \tag{3}$$

where the subscript $\boldsymbol{k}$ specifies the channel, e.g., energy $E_{\boldsymbol{k}}$ and asymptotic momentum $\boldsymbol{k}$.

To obtain an understanding of the physical meaning of $|\psi_{\boldsymbol{k}}^-\rangle$, we form a wave packet centered around this stationary state [20]

$$|\Psi_{\boldsymbol{k}}^-(t)\rangle = \sum_{\boldsymbol{k}'} c_{\boldsymbol{k}'} e^{-iE_{\boldsymbol{k}'}t}|\psi_{\boldsymbol{k}'}^-\rangle, \tag{4}$$

where the index $\boldsymbol{k}'$ specifies energy and asymptotic momentum, and where each $|\psi_{\boldsymbol{k}'}^-\rangle$ is a solution of Eq. (3). The coefficients $c_{\boldsymbol{k}'}$ only attain nonvanishing values for subscripts $\boldsymbol{k}'$ close to $\boldsymbol{k}$. Likewise, we construct a wave packet from the solutions of the reference system centered also at $\boldsymbol{k}$ and with expansion coefficients as in Eq. (4),

$$|\Phi_{\boldsymbol{k}}(t)\rangle = \sum_{\boldsymbol{k}'} c_{\boldsymbol{k}'} e^{-iE_{\boldsymbol{k}'}t}|\phi_{\boldsymbol{k}'}\rangle, \tag{5}$$

with $|\phi_{\boldsymbol{k}'}\rangle$ eigenstates of the reference system, $H_0|\phi_{\boldsymbol{k}'}\rangle = E_{\boldsymbol{k}'}|\phi_{\boldsymbol{k}'}\rangle$. Now, following the procedure in Ref. [20], we insert the complete set of reference states in Eq. (3) between the inverse operator and V and we take the limiting procedure $t\to\infty$ using the relation $\lim_{t\to\infty}\lim_{\eta\to 0^+} e^{i\omega t}/(\omega+i\eta) = 0$ to obtain the late time behavior of the out wave packet

$$\lim_{t\to\infty}|\Psi_{\boldsymbol{k}}^-(t)\rangle = |\Phi_{\boldsymbol{k}}(t)\rangle. \tag{6}$$

Equation (6) shows explicitly that at large times the wave packet centered around the scattering state $|\psi_{\boldsymbol{k}}^-\rangle$ turns into a packet made up of eigenstates of the reference Hamiltonian H_0. In particular the distribution over amplitudes remains unaffected: The coefficients $c_{\boldsymbol{k}'}$ are equal in Eqs. (4) and (5). This is a result which has important consequences for the present discussion. Going back to Eq. (2), we see why. The index $\boldsymbol{k}'$ specifies energy and asymptotic momentum, and we have shown that the distribution over this index is the same in the wave packet constructed from a superposition of exact scattering states and in the wave packet formed by the unperturbed reference states. Hence, we are naturally led to the assumption that by letting the exact wave packet solution of the problem in the right-hand side of Eq. (2) evolve to large times we may perform the projection on reference states in order to obtain the energy and angle resolved spectrum, i.e., one might suspect that $dP/d\boldsymbol{k} = |\langle\psi_{\boldsymbol{k}}^-|\Psi(t_0)\rangle|^2 = \lim_{t\to\infty}|\langle\phi_{\boldsymbol{k}}|\Psi(t_0+t)\rangle|^2$. This relation, however, is incorrect because it does not account correctly for the nonorthogonality of the bound-state spectrum of H and the continuum states of H_0. What is true, however, is that the exact scattering state is obtained from the reference state by application of the Møller or wave operator[20–24]

$$|\psi_{\boldsymbol{k}}^-\rangle = \Omega^-|\phi_{\boldsymbol{k}}\rangle, \tag{7}$$

where $\Omega^- = \lim_{t\to\infty} e^{iHt}e^{-iH_0t}$ projects the states in the continuum of the reference Hamiltonian H_0 onto the correspond-

ing elements in the continuum of H. To stress this fact, we include explicitly the projection on the continuum scattering states of H, $\mathcal{P}_H^{\text{cont}} = \int d\boldsymbol{k} |\psi_{\boldsymbol{k}}^-\rangle\langle\psi_{\boldsymbol{k}}^-|$ in Eq. (7), i.e.,

$$|\psi_{\boldsymbol{k}}^-\rangle = \mathcal{P}_H^{\text{cont}} \Omega^- |\phi_{\boldsymbol{k}}\rangle. \tag{8}$$

Inserting this expression and the definition of the wave operator into Eq. (2), we obtain

$$\frac{dP}{d\boldsymbol{k}} = \lim_{t\to\infty} |\langle \phi_{\boldsymbol{k}} | e^{iH_0 t} e^{-iHt} \mathcal{P}_H^{\text{cont}} | \Psi(t_0)\rangle|^2. \tag{9}$$

Finally, we use the completeness relation $1 = \mathcal{P}_H^{\text{cont}} + \Lambda$, with $\Lambda = \Sigma_n |\psi_n^B\rangle\langle\psi_n^B|$ the projection on the bound state part of the spectrum of H, to obtain

$$\frac{dP}{d\boldsymbol{k}} = \lim_{t\to\infty} |\langle \phi_{\boldsymbol{k}} | e^{iH_0 t} e^{-iHt} (1-\Lambda) | \Psi(t_0)\rangle|^2. \tag{10}$$

The goal we are pursuing is to move the time evolution operator to the right and evolve the exact wave-packet forwards in time from t_0. Clearly $[\exp(-iHt), \mathcal{P}_H^{\text{cont}}] = [\exp(-iHt), 1-\Lambda] = 0$. Accordingly, we propagate the full wave packet from time t_0 to t and project out the bound state part of $|\Psi(t_0+t)\rangle$ to obtain the continuum part $|\Psi'(t_0+t)\rangle = (1-\Lambda)|\Psi(t_0+t)\rangle$ of the wave packet, and the differential ionization probability reads

$$\frac{dP}{d\boldsymbol{k}} = \lim_{t\to\infty} |\langle \phi_{\boldsymbol{k}} | \Psi'(t_0+t)\rangle|^2, \tag{11}$$

which is the formally exact relation justifying the approach proposed in the present paper. Basically, Eq. (11) shows that if the continuum part of the exact wave-packet solution may be propagated long enough after the end of the short laser pulse, then there is no need to construct the exact outgoing scattering states. The angle and energy resolved spectrum may be obtained by projection on the much simpler reference states $|\phi_{\boldsymbol{k}}\rangle$.

In the next sections, we shall discuss from a more practical point of view how the above ideas can be implemented in a numerical calculation. For example, the bound state part is excluded by reference to spatial separation. As we shall see the reference projection states of H_0 can be chosen as analytically known functions. All the phase shifts and information about the short-range behavior of the interaction potential V is in the wave packet $|\Psi(t_0+t)\rangle$.

IV. SCATTERING ANALYSIS IN THE ASYMPTOTIC REGION: FREE ZONE

In this section we write the total field-free Hamiltonian as $H = H_0 + V$, where $H_0 = p^2/2$ is the kinetic energy part and where V denotes the interaction potential [see Fig. 1(c)]. It is assumed that the wave packet is propagated for a time T after the pulse large enough to ensure that even the slowest continuum components of interest have reached asymptotic distances where the potential V can be neglected. In a laboratory experiment long-range Coulomb forces are shielded by the environment at sufficiently large distances so the assumption of a finite range is automatically fulfilled. In a theoretical grid calculation, there is an asymptotic regime where the Coulomb field is small compared with the kinetic energy of the outgoing electron. Slightly more quantitatively, one may consider the drop-off of the Coulomb-induced logarithmic phase distortion of the phase of the outgoing wave, $\eta \ln(2kr)$compared with the free kr behavior, with $\eta = Z/k$ and Z the nuclear charge. If this ratio $\alpha = \eta \ln(2kr)/kr$ is small, the interaction V may be neglected compared with H_0. For example, $\alpha = 0.13$ for $k = 0.1$ a.u., $Z = 1$, and $r = 3200a_0$. This means that large boxes and long propagation times are needed to reach the asymptotic free zone. In gauging the practicality one should of course also consider the complications in determining the exact scattering states entering Eq. (2). Note also that recently box radii of $\sim 1000a_0$ were considered for strong-field ionization of atoms described in the single-active electron model [25]. Hence large boxes are often used in practical calculations and therefore the asymptotic regimes may be available on the numerical grid.

A momentum component $\boldsymbol{k}$ of the wave packet $\Psi(\boldsymbol{r},t)$ will reach the asymptotic regime, say beyond r_0, where the Hamiltonian is described by $H = H_0$ at a time $\sim r_0/k$. In this region $r > r_0$, the eigenstates corresponding to the Hamiltonian H_0 are simply momentum eigenstates $\langle \boldsymbol{r} | \phi_{\boldsymbol{k}} \rangle = (2\pi)^{-3/2} \exp(i\boldsymbol{k}\cdot\boldsymbol{r})$ and the associated projection operator is $\mathcal{P}_{\boldsymbol{k}} = |\phi_{\boldsymbol{k}}\rangle\langle\phi_{\boldsymbol{k}}|$. This means that in this free zone, at a time $T \geq r_0/k$ sufficiently large that the momentum component of interest has arrived, the differential ionization probability is found by projection on plane wave states

$$\frac{dP}{d\boldsymbol{k}} = |\langle \phi_{\boldsymbol{k}} | \Psi'(t_0+T)\rangle|^2. \tag{12}$$

The prime on the time-dependent wave packet indicates that the part of the wave packet not in the asymptotic regime with well-defined plane wave projection operators has been projected away. This is necessary since the plane wave and the eigenstates formally forming the wave packet belong to the spectra of two different Hamiltonians, H_0 and H, respectively, and hence the eigenfunctions are not orthogonal, i.e., $\langle \phi_{\boldsymbol{k}} | \psi_n \rangle$ is generally different from zero. The formal justification for this projection method was given in Sec. III in terms of the wave or Møller operator, which acts only on the continuous spectrum. In Eq. (12) it is the superposition of eigenstates in the wave packet $\Psi'(\boldsymbol{r}, t_0+T)$ that ensures the spatial localization of the continuum components at asymptotic distances, $r > r_0$ at large times, and hence the underlying physical reason why the proposed scattering analysis is well justified and exact. Without details and formal justification the approach discussed here was used recently in the high-frequency regime to described ionization of H_2^+ [26].

The partial wave expansion of the momentum normalized plane wave $\phi_{\boldsymbol{k}}(\boldsymbol{r})$ describing the free final state reads [27]

$$\phi_{\boldsymbol{k}}(\boldsymbol{r}) = \sum_{\ell=0}^{\infty} \sum_{m=-\ell}^{\ell} \sqrt{\frac{2}{\pi}} i^{\ell} j_{\ell}(kr) Y_{\ell m}^{\star}(\hat{\boldsymbol{k}}) Y_{\ell m}(\hat{\boldsymbol{r}}), \tag{13}$$

where $j_{\ell}(kr)$ is a spherical Bessel function and $Y_{\ell m}$ are spherical harmonics. If as in, e.g., our recent approaches

[9,11,12], the wave packet is expanded in partial waves, $\Psi(\boldsymbol{r},t=t_0+T)=\Sigma_{\ell,m}[f_{\ell m}(r,t)/r]Y_{\ell m}(\hat{\boldsymbol{r}})$, the insertion of Eq. (13) into Eq. (12) leads to

$$\frac{dP}{d\boldsymbol{k}} = \left| \sum_{\ell m} \sqrt{\frac{2}{\pi}} i^{-\ell} Y_{\ell m}(\hat{\boldsymbol{k}}) \int_{r_0}^{\infty} j_\ell(kr) f_{\ell m}(r,t_0+T) r dr \right|^2. \tag{14}$$

Equation (14) is easily evaluated numerically since the $f_{\ell m}(r,t)$ are available on the grid and only a one-dimensional integral is involved. As seen from Eq. (14) the projection out of bound states is implemented by integrating radially only from r_0 and outwards.

V. SCATTERING ANALYSIS IN THE MONOPOLE REGIME: COULOMB ZONE

In this section we discuss the most practical way of performing scattering analysis in grid-based wave-packet calculations. For single ionization of atoms, it is clear that the region where the full Hamiltonian is well described by $H_0=p^2/2-Z/r$ is reached when the continuum electron is outside the electronic cloud associated with the other bound state electrons. In many cases this already happens at $\sim 10a_0$. For molecules, the situation is slightly more complicated due to the multicenter character of the problem. The generic features of the problem introduced by the additional nuclei are illustrated already for the molecular potential corresponding to the H_2^+, $V^M(\boldsymbol{r};\boldsymbol{R})=-1/|\boldsymbol{r}-\boldsymbol{R}/2|-1/|\boldsymbol{r}+\boldsymbol{R}/2|$. A multipole expansion of V^M at distances r larger than the internuclear separation R gives $V^M(\boldsymbol{r};\boldsymbol{R})=-2\Sigma_{L\ \mathrm{even}}\frac{(R/2)^L}{r^{L+1}}P_L(\cos\theta)$, so the leading terms are $V^M(\boldsymbol{r},R)\simeq -(2/r)[1-(R/(2r))^2 P_2(\cos\theta)]$; where $P_L(\cos\theta)$ are the Legendre polynomials and the polar axis is parallel to the internuclear axis. For more general molecules, also odd multipoles are allowed and therefore the leading correction to the monopole in the Coulomb zone is the dipole$\sim 1/r^2$. The parameter $\alpha'=1/r$ is hence a measure of the strength of the dipole compared with the monopole. At a radius of $r_0'=100a_0$ it appears to be a quite accurate approximation to ignore higher-order corrections; for H_2^+, $r_0'=100a_0$ makes the approximation excellent. It is hence clear that there exists an intermediate Coulomb zone in space $r>r_0'$, with $r_0'<r_0$ where the monopole from the atomic or molecular system dominates [see Fig. 1(b)]. In this zone the projection operators corresponding to the asymptotic momentum $\boldsymbol{k}$ are known analytically in terms of Coulomb waves $|\psi_{\boldsymbol{k}}^{-,C}\rangle$, $\mathcal{P}_{\boldsymbol{k}}=|\psi_{\boldsymbol{k}}^{-,C}\rangle\langle\psi_{\boldsymbol{k}}^{-,C}|$, and for $r>r_0'$, the ionization probability may be calculated as

$$\frac{dP}{d\boldsymbol{k}} = |\langle\psi_{\boldsymbol{k}}^{-,C}|\Psi'(t_0+T')\rangle|^2. \tag{15}$$

Here, as in Eq. (12), the prime on the wave packet indicates that only the part of the wave packet localized at distances $r>r_0'$ with $H\simeq H_0=p^2/2-Z/r$ is involved. The prime on the additional propagation time T' indicates that now, for the same problem, $T'<T$ where T corresponds to the propagation time needed to reach the asymptotic free zone. The formula in Eq. (15) is very general and highly applicable since in practice quite small r_0' values (20–50 a_0) are large enough, which is a fact that limits the demands on computational time and box size. This is a huge advantage compared with the scattering analysis discussed in Sec. II where new scattering wave functions have to be constructed for each system at hand—the Coulomb waves are analytical and universal. Explicitly, in an expansion in partial waves, the outgoing part of the momentum normalized Coulomb wave function $\psi_{\boldsymbol{k}}^{-,C}(\boldsymbol{r})$, normalized to the $\boldsymbol{k}$ scale, reads [27]

$$\psi_{\boldsymbol{k}}^{-,C}(\boldsymbol{r}) = \sum_{\ell m} \sqrt{\frac{2}{\pi}} i^\ell e^{-i\sigma_\ell} \frac{F_\ell(kr,\eta)}{kr} Y_{\ell m}^\star(\hat{\boldsymbol{k}}) Y_{\ell m}(\hat{\boldsymbol{r}}), \tag{16}$$

with F_ℓ the regular Coulomb function, and $\sigma_\ell(k)=\arg[\Gamma(\ell+1+i\eta)]$ the Coulomb phase shift expressed in terms of the complex Gamma function Γ. With the continuum wave packet $\Psi'(\boldsymbol{r},t)$ expanded in partial waves as in Sec. IV, the momentum resolved probability is

$$\frac{dP}{d\boldsymbol{k}} = \left| \sum_{\ell m} \frac{1}{k} \sqrt{\frac{2}{\pi}} i^{-\ell} e^{i\sigma_\ell} Y_{\ell m}(\hat{\boldsymbol{k}}) \times \int_{r_0'}^{\infty} F_\ell(kr,\eta) f_{\ell m}(r,t_0+T') dr \right|^2. \tag{17}$$

We illustrate the usefulness of Eq. (17) in Sec. VI, where we consider the case of strong-field ionization of H_2^+. In Eq. (17) the radial integral is from r_0' and effectuates the projection out of the bound states. Note that in the limit $\eta\to 0$: $F_\ell(kr)\to krj_\ell(kr)$, $\sigma_l\to 0$, and Eq. (17) turns into Eq. (14) corresponding to the high-energy limit and/or large r or negative ions.

VI. RESULTS AND DISCUSSION

To illustrate the method, we consider strong-field ionization of H_2^+. The field is linearly polarized along the internuclear axis with peak intensity 2×10^{13} W/cm^2, photon energy 0.8 a.u., and a duration of 10 cycles. The envelope of the field is taken to be a sine square and the carrier-envelope phase difference (CEPD) is zero. For the ten-cycle pulse considered here the results are insensitive to the value of the CEPD. Note that the ionization potential is 1.1 a.u. corresponding to the two-photon ionization regime. The frequency of the source can, e.g., be obtained from a free-electron laser source. We expand the time-dependent wave function in spherical harmonics and solve the time-dependent Schrödinger equation by the split-step method discussed in detail elsewhere [9–11]. The maximum angular momentum is $\ell_{\max}=11$, the radius of the sphere in which the calculation is performed is $r_{\max}=300$ a.u., the number of grid points in the radial coordinate is 2048, and the time increment is $\delta t=0.005$ a.u.

To construct the scattering states of H_2^+ at equilibrium distance ($R=2$), we expand the continuum states as

$$\psi_{\mathbf{k}}^{-}(\mathbf{r}) = \sum_{\ell=0}^{\infty} \sum_{m=-\ell}^{\ell} i^{\ell} e^{-i\sigma_\ell} \frac{\phi_{\ell,m}^{k,-}(r)}{r} Y_{\ell m}(\hat{\mathbf{k}}), \tag{18}$$

with σ_ℓ defined after Eq. (16). The function $\phi_{\ell,m}^{k,-}(\mathbf{r})$ is expanded in spherical harmonics and the radial part in turn is expanded in a B-splines basis set [28,29]. The scattering states are calculated applying the inverse iteration method described in Refs. [7,30]. In this way we first obtain wave functions $\phi_{\ell,m}^{k}(\mathbf{r})$ with the K-matrix asymptotic boundary condition

$$\phi_{\ell,m}^{k}(\mathbf{r}) \sim \sum_{\ell' \geq |m|} [F_{\ell'}(kr,\eta)\delta_{\ell',\ell} + K_{\ell,\ell'}^{m}(E) G_{\ell'}(kr,\eta)] Y_{\ell',m}(\hat{\mathbf{r}}), \tag{19}$$

with F_ℓ and G_ℓ the regular and irregular Coulomb wave functions. With the sign convention followed here, the asymptotic forms of the Coulomb waves are $F_\ell \sim \sin\theta_\ell$ and $G_\ell \sim \cos\theta_\ell$, $\theta_\ell = kr - \eta \ln 2kr - \ell\pi/2 + \sigma_\ell$. To obtain the correct out state with incoming spherical wave boundary condition, we change to the S-matrix representation

$$\phi_{\ell,m}^{k,-}(\mathbf{r}) = \sum_{\ell' \geq |m|} [\boldsymbol{I} + i\boldsymbol{K}^{m}(E)]^{-1}_{\ell,\ell'} \phi_{\ell',m}^{k}(\mathbf{r}). \tag{20}$$

In terms of the B-splines basis, the result in Eq. (20) is expressed as

$$\phi_{\ell,m}^{k,-}(\mathbf{r}) = \sum_{\ell' \geq |m|} \sum_{i} c_{\ell\ell' m}^{-,i}(E) B_i(r) Y_{\ell',m}(\hat{\mathbf{r}}), \tag{21}$$

where B_i denotes the ith B-spline of order 10 defined in a box of size of 300 a.u. with a linear breakpoint sequence of 2048 equidistant points in which the first B-spline is deleted from the basis set and the last one is retained (i.e., $N_\ell = 2055$ B splines per angular momentum). The spatial grids coincide in the wave packet and in the B-spline calculation. The partial wave expansion in the B-spline calculation also includes angular momenta up to $\ell_{\max} = 11$. In order to perform the projection [Eq. (2)] over the continuum states of the H_2^+ molecule we rewrite the time-dependent radial wave functions $f_{\ell m}(r;t_0)$ (just after the end of the pulse at t_0) in terms of the same B-splines basis set, i.e,

$$f_{\ell m}(r;t_0) = \sum_{i}^{N_\ell} b_{\ell m}^{i}(t_0) B_i(r), \tag{22}$$

where $b_{\ell m}^{i}(t_0)$ are complex amplitudes since $f_{\ell m}(r;t_0)$ is complex. The evaluation of the scalar products is performed in the B-spline basis and involves matrix-vector operations. The fully differential ionization probability obtained by projection on numerical scattering states of H_2^+ is given by

$$\frac{dP}{d\mathbf{k}}(t_0) = \left| \sum_{\ell m} i^{-\ell} e^{i\sigma_\ell} I_{\ell m}^{-}(E;t_0) Y_{\ell,m}(\hat{\mathbf{k}}) \right|^2, \tag{23}$$

where

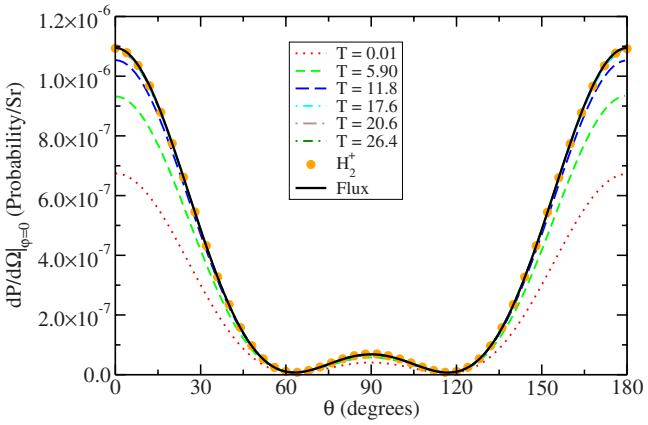

FIG. 2. (Color online) Photoelectron angular distribution for strong-field two-photon ionization of H_2^+ at the equilibrium distance by a linearly polarized laser field with polarization along the direction of the internuclear axis. The azimuthal angle is zero (see text). The field has peak intensity 2×10^{13} W/cm^2, photon energy 0.8 a.u., and a duration of 10 cycles. The envelope of the field is taken to be a sine square. The full curve shows the angular distribution obtained by flux analysis [Eq. (25)] and by projection on the exact H_2^+ scattering states [Eqs. (2) and (23)]. The other curves show snapshots of the projection on single-center Coulomb waves $Z=2$ [Eq. (17)] at different instants of time T after the end of the pulse. The inner boundary of the Coulomb zone is $r_0'=40$ a.u. On the scale of the figure there is no difference between the results obtained by the single-center Coulomb projector applied at $T=17.6, 20.6, 26.4$ a.u., by the flux analysis and by the H_2^+ projector.

$$I_{\ell m}^{-}(E;t_0) = \sum_{\ell'}^{\ell_{\max}} \sum_{i}^{N_\ell} \sum_{j}^{N_\ell} [c_{\ell\ell' m}^{-,i}(E)]^{\star} O_{i,j} b_{\ell' m}^{j}(t_0) \tag{24}$$

is the continuum projection matrix element associated with partial wave ℓ normalized to the S-matrix, consistent with the time-dependent representation of the photoionization process [18,31,32], $O_{i,j} = \int_0^{r_{\max}} B_i(r) B_j(r) dr$ is the overlap matrix, $c_{\ell\ell' m}^{-,i}(E)$ are the coefficients that define the continuum partial wave ℓ [Eq. (21)], $b_{\ell' m}^{j}(t_0)$ the coefficients entering Eq. (22), and m designates the value of the projection of the angular momentum over the molecular axis. We note that the results are insensitive to the time t_0 since the field-free Hamiltonian does not induce coupling between the field-free eigenstates. We keep the argument t_0 in the differential probability as a parameter stressing that the projection on eigenstates is performed immediately after the end of the pulse at time t_0. Also note that the spatial integrals are over the entire region $r \in [0, r_{\max}]$.

In Fig. 2 we show the photoelectron angular distribution, i.e., the quantity $dP/d\Omega = \int (dP/d\mathbf{k}) k^2 dk$, for two-photon ionization of H_2^+ by the field described previously. For the present orientation of the molecular axis with respect to the field there is rotational symmetry around the molecular axis and the angular distribution is the same for all values of azimuthal angle. In the figure we have chosen this angle to be 0. The full curve shows the angular distribution obtained by (i) projection on the exact H_2^+ scattering states [Eqs. (2)

and (23)] and (ii) flux analysis [Eq. (25)] [12]. The latter case (ii) is analyzed with reference only to the grid. We simply evaluate the probability current at the distance $r_{\text{flux}}=200$ a.u. in the direction $\hat{\boldsymbol{k}}$, and integrate over time up to time $T=500$ a.u. after the end of the pulse when all radial outgoing flux has passed the point of observation (see, e.g., Ref. [12]). We obtain the angular distribution from the formula

$$\frac{dP}{d\Omega}(\Omega,T)=\int_{t_0}^{t_0+T}dt' r_{\text{flux}}^2 j_r(r_{\text{flux}},\Omega,t'), \tag{25}$$

with $j_r(\boldsymbol{r},t)=\text{Im}[\Psi^\star(\boldsymbol{r},t)\hat{\boldsymbol{r}}\cdot\boldsymbol{\nabla}\Psi(\boldsymbol{r},t)]$. On the scale of Fig. 2 we see no difference between the results obtained by flux analysis and the scattering-state-projection method confirming that both methods are accurate. The other curves in Fig. 2 show snapshots of the projection on single-center Coulomb waves with $Z=2$ [Eq. (17)] at different instants of time T after the end of the pulse as detailed in the inset. In this calculation we followed the procedure discussed in Secs. III and V and projected out the bound state part of the wave packet. The inner boundary of the Coulomb zone is $r_0'=40$ a.u., i.e., the radial integrals are performed from 40 to 300 a.u. [Eq. (17)]. We see, in accordance with the discussion in the preceding sections, that the results based on the analysis in the Coulomb zone converges to the exact result: On the scale of the figure there is no difference between the results obtained by the single-center Coulomb projector applied at $T=17.6, 20.6, 26.4$ a.u. and the flux and the H_2^+-projector results. Stability of the quantity of interest with respect to time is hence a sign of convergence in the application of the asymptotic projector method. Compared with the flux analysis where a propagation time of $T=500$ a.u. was needed much less propagation time is required with the projection method as seen from the insert in Fig. 2—the result is fully converged at $T=17.6$ a.u.

We note that the angular distribution and the full momentum distribution are much more delicate tests of the accuracy of the theory than, e.g., the photoelectron energy spectrum. The reason is that the former quantities depend on the relative phases between the different partial waves making up the continuum wave functions while the latter is insensitive thereof.

We now turn to the differential momentum distribution. This quantity cannot be obtained by the flux analysis used above nor through the autocorrelation function [11]. A projection method seems to be the only practical method. Figure 3 shows the differential momentum distribution $dP/d\boldsymbol{k}$ for strong-field two-photon ionization of H_2^+ by the same pulse used to obtain the results shown in Fig. 2. The horizontal axis shows the component $k_\parallel$ parallel with the linear polarization. The vertical axis shows a component $k_\perp$ perpendicular to the polarization axis. The momentum distribution is rotationally invariant with respect to the $k_\perp=0$ axis. Figure 3(f) shows the momentum distribution obtained by projection on the H_2^+ scattering states [Eqs. (2) and (23)]. The other distributions show snapshots of the projection on single-center Coulomb waves $Z=2$ at different instants of time T after the end of the pulse [Eq. (17)]. We see that the projection on the single-center Coulomb wave functions in the Coulomb zone converges to the correct numerical result of Fig. 3(f) for increasing T, and hence the figure provides another example for the practicality and accuracy of the present method.

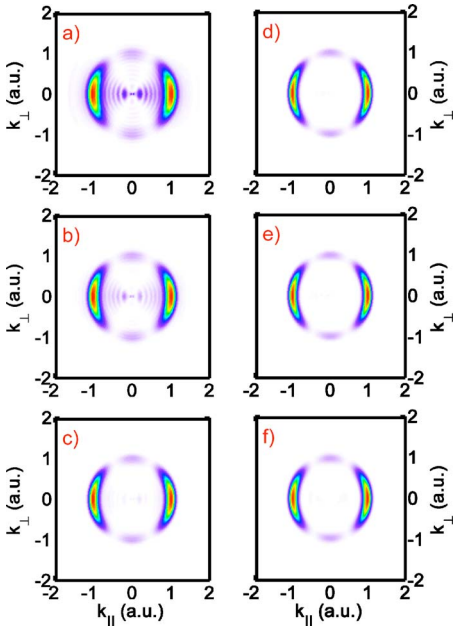

FIG. 3. (Color online) Differential momentum distribution $dP/d\boldsymbol{k}$ for two-photon ionization of H_2^+ by the linearly polarized laser field used in Fig. 2 with polarization along the direction of the internuclear axis. The horizontal axis shows the component $k_\parallel$ parallel with the linear polarization. The vertical axis shows a component $k_\perp$ perpendicular to the polarization axis. The distribution is invariant with respect to rotations around the $k_\perp=0$ axis. The field is as in Fig. 2. Panel (f) shows the momentum distribution obtained by projection on the H_2^+ scattering states [Eqs. (2) and (23)]. The other distributions show snapshots of the projection on single-center Coulomb waves $Z=2$ [Eq. (17)] at different instants of time T after the end of the pulse (a) $T=0.01$ a.u., (b) $T=5.9$ a.u., (c) $T=11.8$ a.u., (d) $T=20.6$ a.u., and (e) $T=26.4$ a.u.. The inner boundary of the Coulomb zone is $r_0'=40$ a.u.

VII. THE TWO-ELECTRON PROBLEM

In this section we propose the extension to two-electron systems. An accurate description of two-electron systems and in particular the helium atom under time-dependent strong fields has been a quest for theory in the last 10–15 years [33].

A. Single ionization and excitation

The channel corresponding to single ionization and excitation of He is readily resolved by the projection operator $\mathcal{P}_{\boldsymbol{k}_1}\otimes\mathcal{P}_{n_2}$ where $\mathcal{P}_{\boldsymbol{k}_1}=|\Phi_{\boldsymbol{k}_1}\rangle\langle\Phi_{\boldsymbol{k}_1}|$ is the projection operator of the appropriate reference system (see Sec. III) that "measures" one of the electrons in the asymptotic momentum $\boldsymbol{k}_1$. The operator $\mathcal{P}_{n_2}=|\Phi_{n_2}\rangle\langle\Phi_{n_2}|$ projects on the nth eigenstate of the He^+ subsystem. The advantage here is that both $\mathcal{P}_{\boldsymbol{k}_1}$

and $\mathcal{P}_{n_2}$ are known analytically. So, the proposed formula giving the photoelectron angular distribution with the ion left in the analytical Φ_{n_2} bound state of He^+, and working in the spatial regime where the continuum electron moves in the $-1/r$ Coulomb potential from the screened nuclei, reads

$$\frac{dP}{d\boldsymbol{k}_1}(n_2) = |\langle \psi_{\boldsymbol{k}_1}^{C,-} \Phi_{n_2} | \Psi'(t_0 + T') \rangle|^2, \tag{26}$$

where $|\psi_{\boldsymbol{k}_1}^{C,-}\rangle$ is a Coulomb wave function with asymptotic momentum $\boldsymbol{k}_1$. In Eq. (26), only the bra or the ket needs to be properly antisymmetrized since the antisymmetrization operator $\mathcal{A}$ is idempotent ($\mathcal{A}^2 = \mathcal{A}$).

B. Double ionization

Recently, works have appeared that focus on the problem of two-photon double ionization (for a recent paper that gives a detailed survey of the literature see Ref. [17]). Multiphoton double ionization is a computationally very hard problem: It involves six spatial dimensions, and infinitely many coupled channels. Also the extraction of scattering information is very complicated. One approach [15,16] is to perform the analysis of the numerical data based on where in space the electron density is localized. An alternative is to generate the multichannel double-continuum wave function [19]. Another method was developed in connection with the time-dependent close-coupling method [34] where the final-state wave function after the pulse was projected on a product of uncorrelated Coulomb wave functions. With this method fully differential cross sections can be obtained. Very recently, an alternative *ab initio* approach relying on the construction of the correlated multichannel scattering wave function by means of the so-called J matrix was developed [17]. In that approach the probability for double ionization was obtained by subtracting from the total wave function the bound-state and single-continuum parts, and no angular differential information was obtained. Hence, it is fair to say that the extraction of scattering information in the double continuum reached by multiphoton absorption is a very challenging problem.

In this section, it is discussed how a straightforward generalization of the ideas of the preceding sections may help in the scattering analysis. An advantage of the proposed method is that only controllable approximations in the measurement projection-operator step are introduced. If propagation to large distances of the wave packet is possible, the presented formula is exact and the final state for the analysis of the two-electron continuum is analytical. Hence, also in this complicated case the grid-based wave-packet calculation need not be supplemented in any way.

In the case of double ionization, a fully differential measurement determines the two momenta $\boldsymbol{k}_1$, $\boldsymbol{k}_2$ of the ejected electrons. Now, as discussed already in connection with the effective two-body Coulomb problem in Sec. V, it is well known that an asymptotic plane wave is inconsistent with the solution to the Schrödinger equation pertaining to the Coulomb problem. The Coulomb tail of the potential generates a logarithmic phase that distorts the plane wave so that the asymptotic momentum $\boldsymbol{k}$ is only reached slowly as r increases. Generalizing to the case of the three-body Coulomb problem with a He^{++} nucleus and two continuum electrons, we expect such logarithmic phase distortions in the relative motion of each pair. Indeed it has been known for a long time (see, e.g., [35] and references therein) that the *exact* form of the wave function describing two electrons in the continuum of an infinitely heavy He^{++} nucleus when all interparticle distances are large is given by

$$\chi^-(\boldsymbol{k}_1,\boldsymbol{r}_1;\boldsymbol{k}_2,\boldsymbol{r}_2) = \frac{1}{(2\pi)^3} e^{i(\boldsymbol{k}_1\cdot\boldsymbol{r}_1 + \boldsymbol{k}_2\cdot\boldsymbol{r}_2)} e^{-i\eta_1 \ln(k_1 r_1 + \boldsymbol{k}_1\cdot\boldsymbol{r}_1)} e^{-i\eta_2 \ln(k_2 r_2 + \boldsymbol{k}_2\cdot\boldsymbol{r}_2)} e^{-i\eta_{12} \ln(k_{12} r_{12} + \boldsymbol{k}_{12}\cdot\boldsymbol{r}_{12})}, \tag{27}$$

where $\eta_j = -Z\mu/k_j$ $(j=1,2)$, $Z=2$, $\eta_{12} = \mu/k_{12}$, $\boldsymbol{k}_{12} = \boldsymbol{k}_1 - \boldsymbol{k}_2$, $\boldsymbol{r}_{12} = \boldsymbol{r}_1 - \boldsymbol{r}_2$. Equation (27) shows that the asymptotic form consists of two phase-distorted plane waves for the two outgoing electrons and an additional phase (last factor) stemming from the electron-electron interaction. Clearly this last phase factor is just as important as the other two, and in particular it has to be included in order to conform with the correct boundary conditions. This means that projections based on a product of two uncorrelated Coulomb wave functions [34] should only be applied with care (see also the discussion in [17]). As in Eq. (26), the projection state needs not be symmetrized.

We note in passing that in the 90's much work was invested into the construction of an analytical three-body Coulomb wave function that satisfied the correct boundary condition of Eq. (27) [36]. The interest was, e.g., in single-photon double ionization in the perturbative regime. The analysis was made in time-independent theory and, accordingly, the wave functions that entered in the construction of the appropriate matrix elements had to be known and defined in all of space: There was no possibility to propagate a wave packet to large interparticle distances and to make the scattering analysis in the asymptotic part of space with the exact state in Eq. (27). In this work, however, this possibility forms the grounds of the proposed method, and therefore we suggest that the analysis of the double continuum may be studied by evaluation of the formula

$$\frac{dP}{d\boldsymbol{k}_1 d\boldsymbol{k}_2} = |\langle \chi_{\boldsymbol{k}_1,\boldsymbol{k}_2}^- | \Psi'(t_0 + T') \rangle|^2, \tag{28}$$

with $\langle \boldsymbol{r}_1, \boldsymbol{r}_2 | \chi_{\boldsymbol{k}_1,\boldsymbol{k}_2}^- \rangle$ given in Eq. (27) and with the continuum part of the wave packet $|\Psi'(t)\rangle$ evaluated at time $t_0 + T'$ where all the particles are far away from each other (r_1, r_2

and r_{12} large). The asymptotic form of Eq. (27) is straightforwardly generalized to the N-particle problem [37] and a generalization to the N-particle breakup of the present approach is therefore formally possible.

The exclusion of the two-electron bound states implied by the prime on the wave packet in Eq. (28) ensures that no artificial result from the single-ionization channel appears in the double-ionization signal. This is easily proved by noting that for bound state components of the singly ionized species of a spatial range similar to the range of the two-electron bound states, the bound state wave function in the single-ionization channel is zero in the integration volume under concern in Eq. (28) and thus implies an overall vanishing overlap between the double ionization projector and the single-ionized channels.

A nice feature of the present approach is that the wave packet includes every interaction of the full Hamiltonian. It is at the level of the measurement projection operator that the approximations are introduced and in a controlled way: The longer propagation time, the more exact result. When the momentum components of interest are in the asymptotic regime then Eq. (27) is valid, and the angle and energy resolved ionization probability of Eq. (28) remains constant in time; a prerequisite for a converged calculation.

VIII. SUMMARY AND CONCLUSION

In conclusion, the theory of measurement projection operators in time-dependent grid-based wave-packet calculations involving continua was discussed. The mathematical foundation of the approach relies on the properties of the wave operators that act on continuum states. A hierarchy of projection operators relevant in their individual restricted configuration spaces was presented. At large distances from the scattering or interaction center the projection operators are simply given in terms of momentum eigenstates. If the wave packet is only propagated to intermediate distances where the Coulombic monopole is significant, the projection operators are generated from Coulomb waves with incoming scattering wave boundary conditions. If propagation of the wave packet to these asymptotic regimes is impeded, the projection operators involve the exact scattering states which are not readily available in the wave-packet calculation and hence must be supplied by an additional calculation. The present work demonstrates that the Coulomb and plane wave states forming the projection operators are conveniently expressed in a spherical coordinate partial wave expansion. However, since the Coulomb and plane wave states are known analytically, it is possible to use the present method in any coordinate grid representation. Therefore, in general time-dependent grid calculations, the present method is potentially very practical since a whole range of processes may be analyzed directly by making the appropriate projections over restricted parts of a numerical grid. There is no need for finding the scattering states for each individual subsystems under study. The accuracy of the method was illustrated by considering strong-field ionization of H_2^+ where the exact scattering states were found by a numerical *ab initio* method.

ACKNOWLEDGMENT

This work was supported by the Danish Research Agency (Grant No. 2117-05-0081).

[1] *Atoms in Intense Laser Fields*, edited by M. Gavrila (Academic Press, San Diego, 1992).
[2] *Molecules in Laser Fields*, edited by A. D. Bandrauk (Marcel Dekker, New York, 1994).
[3] *Molecules and Clusters in Intense Laser Fields*, edited by J. H. Posthumus (Cambridge University Press, Cambridge, 2001).
[4] J. C. Wells, D. R. Schultz, P. Gavras, and M. S. Pindzola, Phys. Rev. A **54**, 593 (1996).
[5] We shall use capital Greek letters for wave packets and small Greek letters for time-independent states.
[6] F. Martin, A. Riera, and I. Sanchez, J. Chem. Phys. **94**, 4275 (1991).
[7] M. Brosolo, P. Decleva, and A. Lisini, Comput. Phys. Commun. **71**, 207 (1992).
[8] S. Selstø, M. Førre, J. P. Hansen, and L. B. Madsen, Phys. Rev. Lett. **95**, 093002 (2005).
[9] T. K. Kjeldsen, L. B. Madsen, and J. P. Hansen, Phys. Rev. A **74**, 035402 (2006).
[10] T. K. Kjeldsen, L. A. A. Nikolopoulos, and L. B. Madsen, Phys. Rev. A **75**, 063427 (2007).
[11] L. A. A. Nikolopoulos, T. K. Kjeldsen, and L. B. Madsen, Phys. Rev. A **75**, 063426 (2007).
[12] L. A. A. Nikolopoulos, T. K. Kjeldsen, and L. B. Madsen, Phys. Rev. A **76**, 033402 (2007).
[13] M. D. Feit, J. A. Fleck, and A. Steiger, J. Comput. Phys. **47**, 412 (1982).
[14] M. R. Hermann and J. A. Fleck, Phys. Rev. A **38**, 6000 (1988).
[15] J. S. Parker, L. R. Moore, K. J. Meharg, D. Dundas, and K. T. Taylor, J. Phys. B **34**, L69 (2001).
[16] J. S. Parker, B. J. S. Doherty, K. J. Meharg, and K. T. Taylor, J. Phys. B **36**, L393 (2003).
[17] E. Foumouo, G. L. Kamta, G. Edah, and B. Piraux, Phys. Rev. A **74**, 063409 (2006).
[18] H. Park and R. N. Zare, J. Chem. Phys. **104**, 4554 (1995).
[19] L. A. A. Nikolopoulos and P. Lambropoulos, J. Phys. B **34**, 545 (2001).
[20] P. Roman, *Advanced Quantum Theory: An outline of the fundamental ideas* (Addison-Wesley, Reading, 1965).
[21] R. G. Newton, *Scattering Theory of Waves and Particles* (McGraw-Hill, New York, 1966).
[22] M. L. Goldberger and K. M. Watson, *Collision Theory* (Wiley, New York, 1964).
[23] T.-Y. Wu and T. Ohmura, *Quantum Theory of Scattering* (Prentice Hall, London, 1962).
[24] D. Yafaev, *Scattering Theory: Some Old and New Problems*, Lecture Notes in Mathematics, Vol. 1735 (Springer, Berlin, 2000).
[25] Z. Chen, T. Morishita, A.-T. Le, M. Wickenhauser, X. M.

Tong, and C. D. Lin, Phys. Rev. A **74**, 053405 (2006).
[26] S. Selstø, J. F. McCann, M. Førre, J. P. Hansen, and L. B. Madsen, Phys. Rev. A **73**, 033407 (2006).
[27] H. Friedman, *Theoretical Atomic Physics*, 2nd ed. (Springer, New York, 1998).
[28] H. Bachau, E. Cormier, P. Decleva, J. E. Hansen, and F. Martín, Rep. Prog. Phys. **64**, 1601 (2001).
[29] C. de Boor, *A Practical Guide to Splines* (Springer, New York, 1978).
[30] M. Brosolo and P. Decleva, Chem. Phys. **159**, 185 (1992).
[31] G. Breit and H. A. Bethe, Phys. Rev. **93**, 888 (1954).
[32] C. Jungen and D. Dill, J. Chem. Phys. **73**, 3338 (1980).
[33] P. Lambropoulos, P. Maragakis, and J. Zhang, Phys. Rep. **305**, 203 (1998).
[34] J. Colgan, M. S. Pindzola, and F. Robicheaux, J. Phys. B **34**, L457 (2001).
[35] M. Brauner, J. S. Briggs, and H. Klar, J. Phys. B **22**, 2265 (1989).
[36] F. Maulbetsch and J. S. Briggs, J. Phys. B **26**, 1679 (1993).
[37] L. Rosenberg, Phys. Rev. D **8**, 1833 (1973).